Composite Structures 168 (2017) 746–757

Contents lists available at ScienceDirect

Composite Structures

journal homepage: www.elsevier.com/locate/compstruct

The study on the morphing composite propeller for marine vehicle. Part I: Design and numerical analysis

Fanlong Chen [a,1], Liwu Liu [a,1], Xin Lan [b], Qinyu Li [a], Jinsong Leng [b], Yanju Liu [a,*]

[a] Department of Astronautical Science and Mechanics, Harbin Institute of Technology, Harbin 150001, People's Republic of China
[b] Centre for Composite Materials and Structures, Harbin Institute of Technology, Harbin 150080, People's Republic of China

ARTICLE INFO

Article history:
Received 25 September 2016
Revised 25 January 2017
Accepted 13 February 2017
Available online 16 February 2017

Keywords:
Smart structure
Morphing composite propeller
Marine vehicles
Transmission mechanism
Hydrodynamic analysis
Structure responses

ABSTRACT

This paper details a novel morphing composite propeller (MCP) to improve the performance for marine vehicles (MVs). A MCP is designed with an active rotatable flap (ARF) to change the blade's local camber with flap rotation. A piezo-stack actuator has been connected with one transmission mechanism housed in the propeller blade to push the ARF to obtain various configuration of the MCP. A commercial Finite Element (FE) software ANSYS Fluent was employed to analyse and simulate the hydrodynamics around the propeller with the ARF ranging from −5° to +5° and the advance speeds ranging from 1.08 to 2.52 m/s. Finally, the FE results has been used to predict improved performances of the MCP and found the morphing composite propeller configuration has improved the efficiency by 1.1% while improving the structural durability.

1. Introduction

One of the most widely used propulsion equipment, the propellers play an essential role on UVs and other underwater vehicles. For the propellers on the MVs, the working conditions are very complicated and many off-design operating conditions will be suffered like crashback or rapid reversing. Therefore, the increased efficiency and the thrust of propellers will benefit their working conditions. Due to these reasons an integrated geometry reconfiguration technique such as morphing composite propeller seems to be capable of improving the efficiency significantly. However, only a few published research work are available on the morphing propellers. In 2000, a biomimetic propulsor based on shape memory alloy (SMA) was fabricated by Bandyopadhyay et al. [1] and the theoretical analysis has presented [2]. In 2005, a morphing propeller based on reconfiguration technique was fabricated by Wasylyszyn [3] in Texas A&M University. In this work a rotatable leading edge (LE) flap actuated by SMA is assembled on the propeller blade and a concise hydrodynamic test has been conducted.

In order to study the hydrodynamic characteristics of a morphing composite propeller of an MV, a proper analytical model and an efficient simulation method are needed. Since the 1980s, the numerical methods of Computational Fluid Dynamics (CFD) have received increasing attentions. Stem et al. [4] have investigated the hydrodynamic characteristics of a submarine propeller and fluid–structure interaction between submarine body and the propeller was calculated with CFD. Abdel-Maksoud et al. [5] have investigated a highly skewed propeller (HSP) using viscous flow theory. Rhee et al. [6] explored the validation of the results calculated by RANS of a marine propeller with unstructured grid. The performances of off-design conditions of marine propeller are calculated by Broglia et al. [7] with CFD theory, and this method was helpful to evaluate the overall performance of various propellers working under off-design conditions. Gaggero et al. [8] utilized the RANS method to analyze the tip vortex cavitation then compared with experiment results, and the comparison has shown a good agreement. Subsequently, Sánchez-Caja et al. [9] improved the calculation accuracy of the propeller wake prediction with RANS method. In order to simulate the cavitation under unsteady state of the marine propeller, Bin Ji et al. combine the partial time-averaged N-S (RANS) method with modified turbulent model to process the simulation [10].

During past few decades many researchers have explored various methods for the numerical analysis of composite marine propellers. In 1996, Lin et al. [11,12] develop the 3D FEM/VLM method combining the effect of fluid-structure interaction (FSI) and then the hydroelastic analysis of the marine propeller. In 2004, Lee et al. [13] improve this method and conduct the

* Corresponding author.
E-mail address: yj_liu@hit.edu.cn (Y. Liu).
[1] These authors contributed equally to this work.

http://dx.doi.org/10.1016/j.compstruct.2017.02.072
0263-8223/

Nomenclature

ARF	active rotatable flap: the deformable component of the propeller
AC	advance coefficient: the dimensionless variable to characterize advance speed
BC	boundary condition
BEM	boundary element method
BWC	blade with cavity
BWoC	blade without cavity
CFD	computational fluid dynamics
CFRP	carbon fiber reinforced plastics
CP	conventional propeller
DM	design modeler
EAP	electro-active polymer: one dielectric smart material whose shape can deform with various voltages
FEM	finite element method
FH	flexure hinge: the flexible linkage of the transmission mechanism as a mechanical hinge does
FSI	fluid-structure interaction
IFF	inner flow field: the computational domain of the inner body who embraces the propeller
IP	interface pair: the adjacent interfaces of the inner body and the outer body of the computational domains
LE	leading edge
MCP	morphing composite propeller: the smart and morphing structure
MRF	multi-reference frame: a simplified model embedded in Fluent to make the calculation more economical with satisfied accuracy
MV	marine vehicle
OFF	outer flow field: the computational domain of the outer body who embraces the iff and the propeller
RANS	Reynolds-averaged Navier–Stokes
SMA	shape memory alloy: one smart material made by alloys
SMP	shape memory polymer: one smart material made by polymers
SMPC	shape memory polymer composite: the combination of SMP and other ingredients which include fibers, functional particles, nano-materials (nanotube or nanoparticles etc.) and so on
SS	stacking sequence
TE	trailing edge
TM	transformation mechanism: the bridge between actuator and ARF, which is used to transmit displacement and driving force
VLM	vortex lattice method

composite layering optimization by means of genetic algorithm. Following their work, the stress and fatigue evaluation of composite propeller has been studied by Lin [14]. From 2007 to 2013, Young et al. [15–20] have developed abundant achievements on propeller design and numerical analysis, especially for the composite propellers. In 2007, Young [15] conducts the time-dependent hydroelastic analysis of cavitating propulsors with a 3-D potential-based boundary element method (BEM) coupled with a 3-D finite element method (FEM). In 2008–2009, Young et al. [16,17] study the fluid–structure interaction of flexible composite propellers in subcavitating and cavitating flows based on the coupled boundary element (BEM) and finite element (FEM) approach at first, and then the self-twisting composite marine propellers under both steady and unsteady operating conditions are calculated. Next, Young et al. [18,19] come up with the analysis of self-adaptive composite marine propeller and explore the scaling law for the flexible propellers. In 2013, Nelson and Young et al. [20] perform a simultaneous optimization of propeller–hull systems, whose destinations result from the energy economical point of view. However, all these contributions rarely referred to the morphing composite propellers as our work does, which is a profound approach for maneuver and durability of marine vehicles.

In conclusion, the various simulations of CFD methods are capable to study the overall performances of the marine propeller ranging from hydrodynamics to wake flow prediction. Through the CFD methods, the satisfied results can be obtained compared with hydrodynamic tests. Thus, in this paper, the RANS method will be adopted to study the hydrodynamic characteristics with the configuration varying with the rotation of ARF, which is also sound and reasonable.

The smart materials can be functionally designed according to intended usage such as, piezoelectric materials with their composites [21–23], magnetostrictive materials [24,25], shape-memory alloy (SMA) [26,27], shape-memory polymers with their composites (SMPs and SMPCs) [28–30], electroactive polymers (EAP) [31,32]. These functionally designed smart materials have revolutionized the fields on sensors and actuators. As a result there are windows of opportunities for researchers and engineers to manufacture smart structures for many engineering applications.

Many research work have shown the potential use of smart materials and structures on helicopter rotors. However, the application of the smart materials and structures on marine propellers are limited. Chopra [33] has introduced the double piezoelectric crystal plates to drive the active flap, and obtain favorable results on decreasing the hub dynamic load of the rotor. Later, Lee and Chopra [34] design and fabricate an L-L actuator based on piezo-stack ceramic, but the result seems not very qualified with their design scheme for some design defects. Andreas et al. [35] have designed a C-shaped actuator, however the dynamic balance problems occur for the structural layout when the rotor undergoes wind tunnel test. Straub et al. [36] have fabricated a double X-shaped actuator, which was performed well during the wind tunnel testing. Qingqing Lu [37] has designed and fabricated a rhombus-shaped actuator based on piezo-stack ceramic, which shows positive effect during the wind tunnel testing.

This paper will explore whether the geometry reconfiguration with active control techniques can improve the performance of a propeller of MV. This propeller will be equipped with an actuator to rotate ARF which will provide propeller's morphing characteristics. Moreover, the morphing propeller has self-adaptive function; i.e. the propeller can achieve different navigation modes, such as lower rotation velocity with higher advance speed, or higher rotation velocity with lower hub/shaft load.

2. The selection of turbulence model

The RANS method is that the turbulence can be simplified as two parts—time-averaged flow and transient fluctuated flow. Based on RANS method, the time-averaged continuum equation and N-S equations are "translated" as follows [38]:

$$\frac{\partial \rho}{\partial t} + \frac{\partial}{\partial x_i}(\rho u_i) = 0 \tag{1}$$

$$\frac{\partial}{\partial t}(\rho u_i) + \frac{\partial}{\partial x_j}(\rho u_i u_j) = -\frac{\partial p}{\partial x_i} + \frac{\partial}{\partial x_j}(\mu \frac{\partial u_i}{\partial x_j} - \rho \overline{u_i' u_j'}) + S_i \tag{2}$$

where $\tau_{ij} = -\rho \overline{u_i' u_j'}$ is the Reynolds stresses.

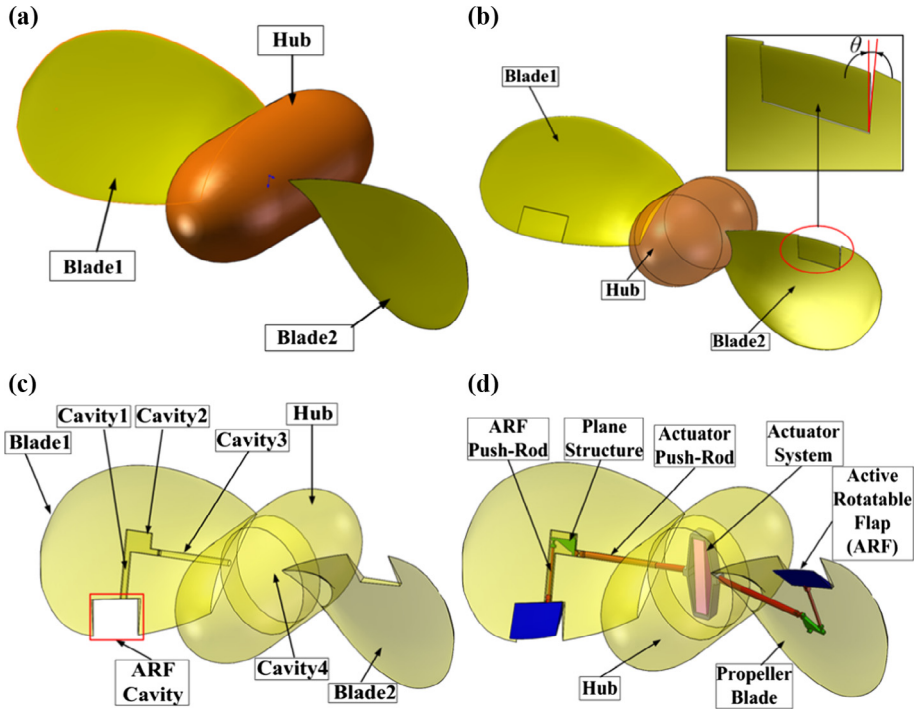

Fig. 1. Schematic of MCP (a) conventional propeller (b) simplification of MCP (c) cavities of MCP (d) ultimate design.

Over the years many researchers have modified this model with some assumptions. According to the different assumptions, the RANS method can be represented by two turbulence models, that is, Reynolds Stress Model and Eddy Viscosity Model. For this research, the Eddy viscosity Model, two-equation model, is mainly utilized as it is convenient and reasonably accurate, namely, the standard $k-\varepsilon$ model is utilized.

3. Structural design of morphing composite propeller (MCP)

Initially, a scaled 1:20 model of a conventional propeller (CP) was modeled using SolidWorks, and subsequently an ARF shape was modelled. The scaled model was selected according to the limitations of available experimental facilities. Next a piezo-stack actuator system is selected and the transmission mechanism (TM) was designed, and the actuator system was assembled into the propeller hub. The TM was placed in the propeller blade and the ARF was linked with propeller blade. The CP is shown in Fig. 1(a), which is composed with three components — one hub and two blades. Based on the CP design scheme, a morphing composite propeller (MCP) assembled with active rotatable flap is designed. Compared with CP, the main distinction is the addition of the ARF, shown as Fig. 1(b). At a cavity on the trailing edge (TE) of the propeller, Fig. 1(c), the ARF connected through the ESS and it can rotate around thus the local camber of the propeller blade can be changed during the operation; the cavity area that the ARF occupies was 0.5R–0.7R (R is the propeller radius) along the reference line of the blade, and the width was approximately 25% of the local propeller width. There were two options for ARF assembly, one is the ARF assembles on the blade near the LE [3] and the other is the ARF embeds on the area near the TE. The former may cause cavitation issue easier than the latter since the water will come upon the LE at first, and the cavitation will exists for the whole process when the water flows along the blade surface. Thus, the second scheme was chosen for design the ARF. The overall design is shown as Fig. 1(d).

Due to the scale of the actuator system was larger than the propeller blade in thickness direction, it was impossible to incorporate the actuator mechanism into the propeller blade. The initial idea was to attach the actuator system in the hub, and the bridge

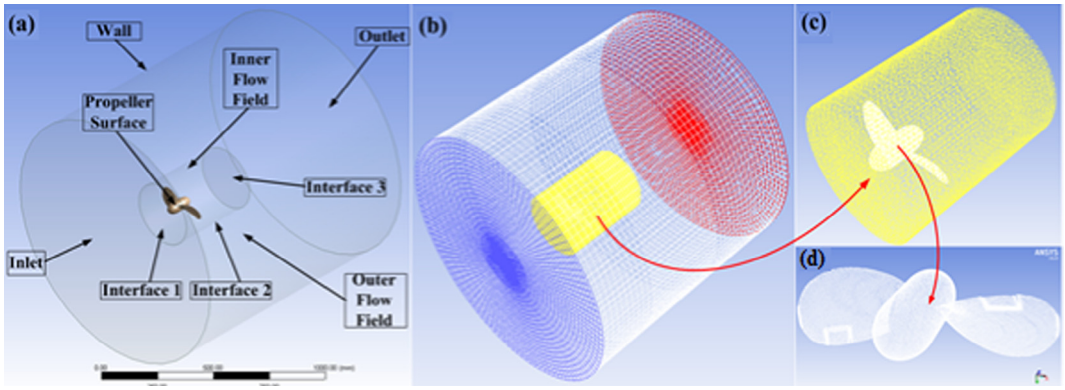

Fig. 2. Definition of outer flow (a) outer flow (b) hybrid mesh (c) unstructured mesh for IFF (d) mesh for MCP.

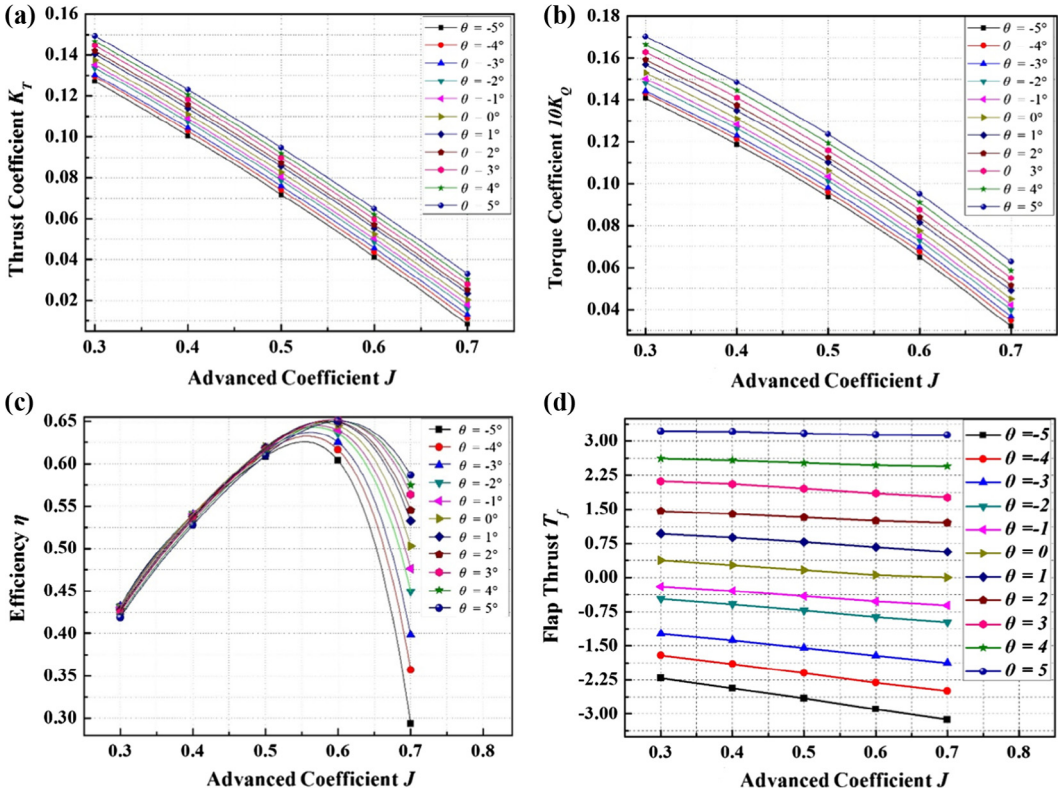

Fig. 3. The analysis curves for first analysis method (a) The K_T – J curves (b) The $10K_Q$ – J curves (c) The η– J curves (d) The T_f –J curves.

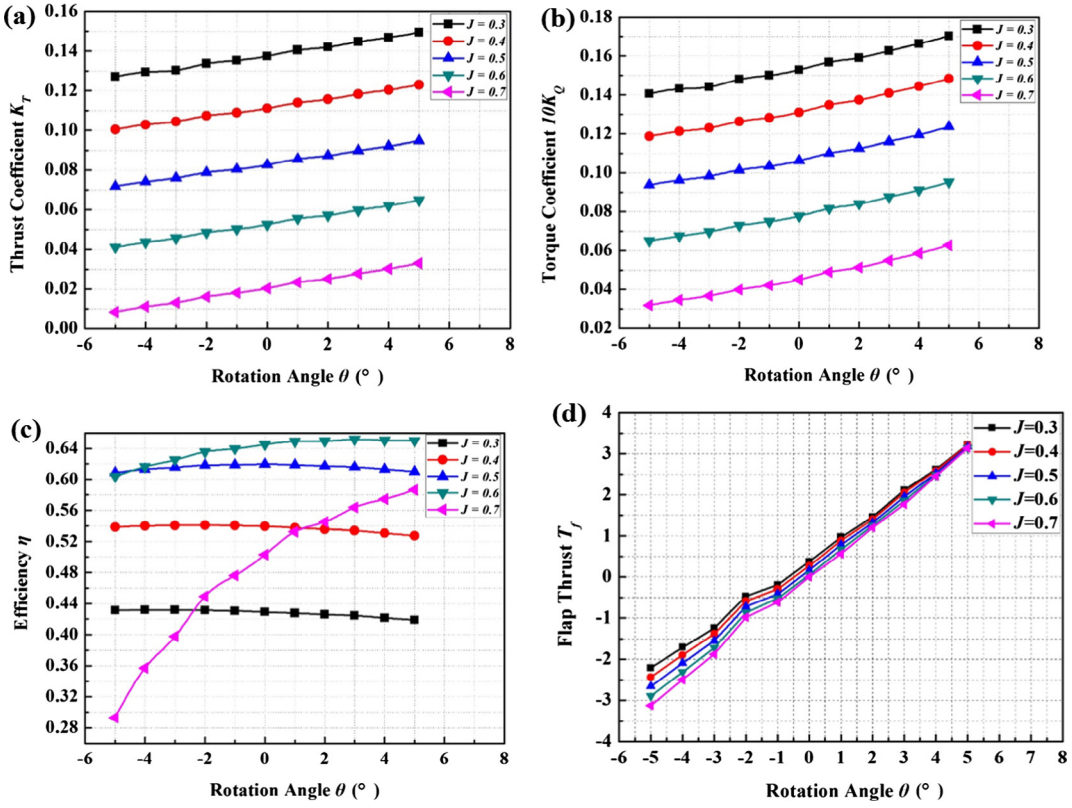

Fig. 4. The analysis curves for second analysis method (a) The K_T –θ curves (b) The $10K_Q$ –θ curves (c) The η– θ curves (d) The T_f – θ curves.

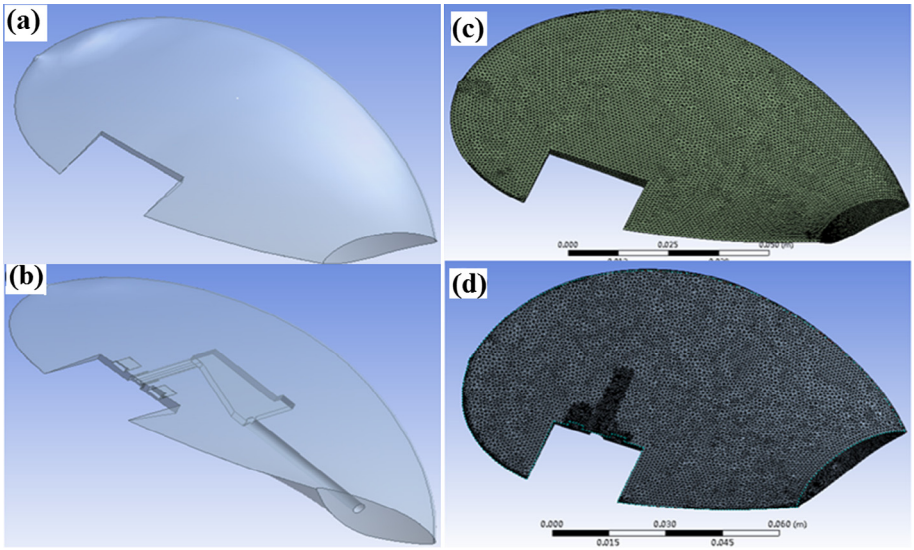

Fig. 5. Modeling for MCP blade with and without cavities (a) geometry without cavities (b) geometry with cavities (c) mesh model without cavities (d) mesh model with cavities.

between the actuator and the ARF is the TM. Nevertheless, the blade e is extremely thin, at the TE; for the concept of TM was not achievable. In order to tackle these obstacles, a novel TM was designed and included in the blade, shown in Fig. 1(d).

4. The hydrodynamic analysis of the MCP

ANSYS Fluent a commercial software will be used for hydrodynamics analysis of MCP. The hydrodynamic analysis of the MCP will be done for various advance speeds and rotation angles of ARF. These performance of the MCP will be compared with the performances of an unmodified blade. Following dimensionless parameters will be calculated using the results from Fluent analysis.

$$\text{Advance coefficient} \quad J = \frac{V}{nD} \tag{3}$$

$$\text{Thrust coefficient} \quad K_T = \frac{T}{\rho n^2 D^4} \tag{4}$$

$$\text{Torque coefficient} \quad K_Q = \frac{Q}{\rho n^2 D^5} \tag{5}$$

$$\text{Efficiency} \quad \eta = \frac{TV}{2\pi nQ} \tag{6}$$

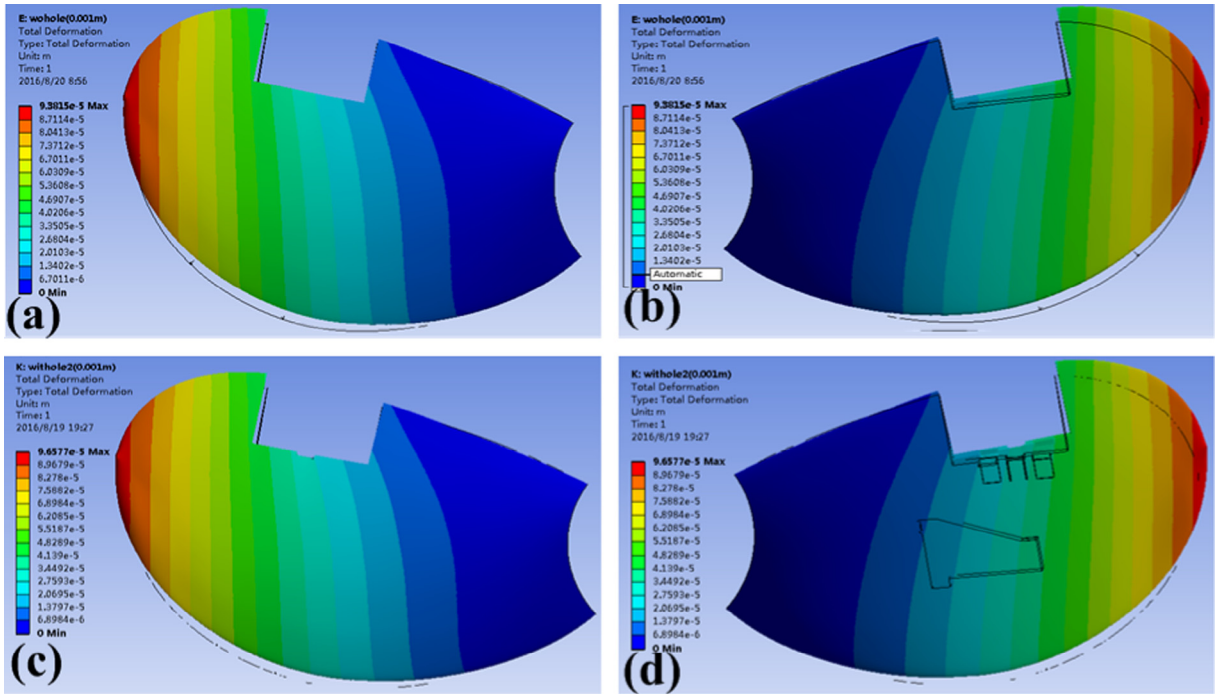

Fig. 6. The deformation contours of the blade with/wo cavity (a) suction surface wo cavity; (b) pressure surface wo cavity; (c) suction surface with cavity; (d) pressure surface with cavity.

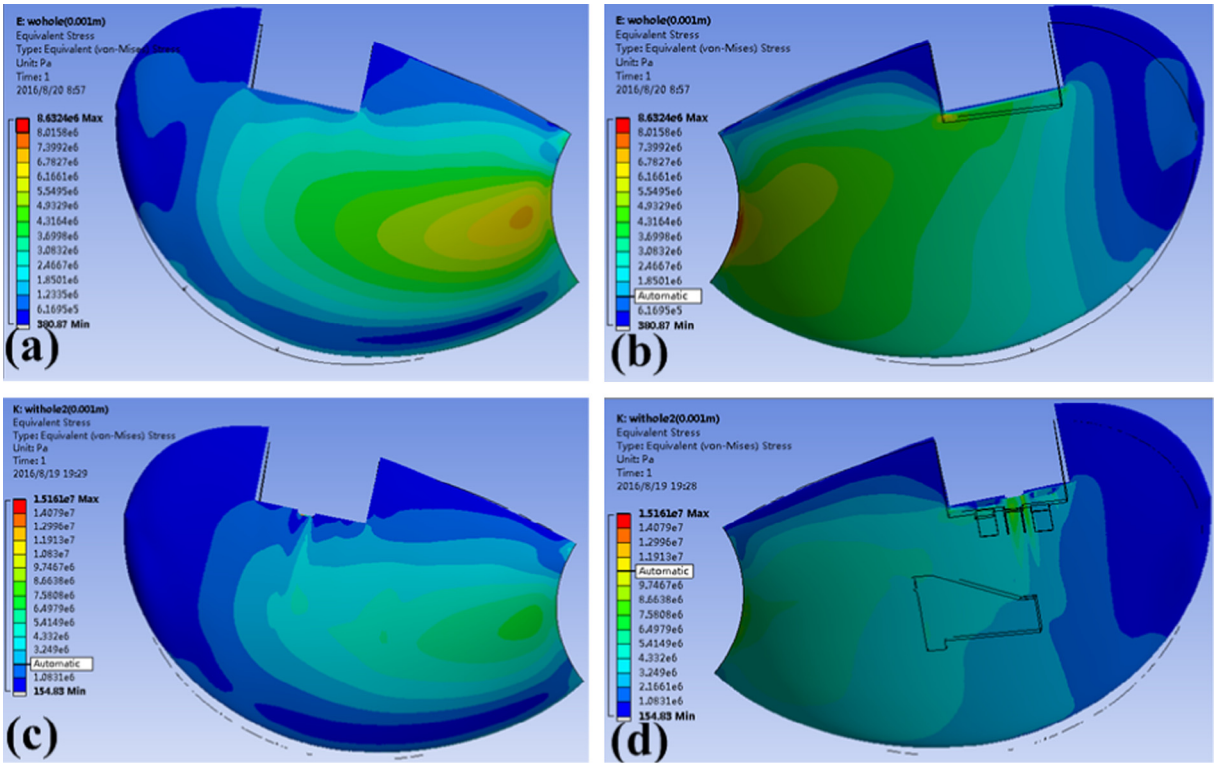

Fig. 7. The stress contours of the blade with/wo cavity (a) suction surface wo cavity; (b) pressure surface wo cavity; (c) suction surface with cavity; (d) pressure surface with cavity.

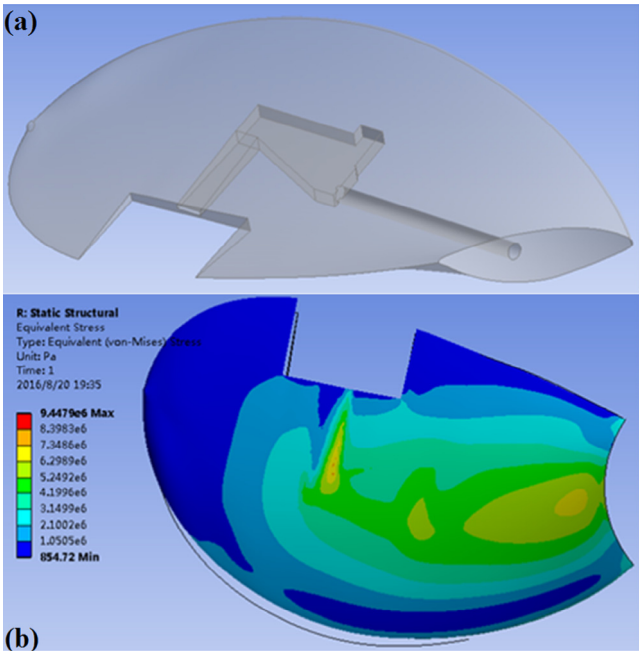

Fig. 8. Geometry and simulation of redesign BWC (a) geometry (b) stress contour.

where

V – advance speed (m/s);
D – diameter of propeller (m);
ρ – water density (998.2 kg/m3);n – rotation velocity (rps);
T – thrust (N);
Q – torque (N·m).

Table 1
The comparison of the two blades (BWoC and BWC).

Resultgeometry	Displacement (max)(mm)	Stress (max)(Mpa)
BWoC	9.38e−2	8.63
BWC (before)	9.66e−2	15.16
BWC (after)	9.55e−2	9.45

Table 2
The parameters of the Carbon/Epoxy uni-directional reinforcement [39].

Parameter type	Denotation	Unit	Value
Young's modulus	E_x	GPa	135
	E_y	GPa	15
	E_z	GPa	15
Shear modulus	G_{xy}	GPa	5
	G_{yz}	GPa	2.9
	G_{xz}	GPa	5.3
Poisson's ratio	v_{xy}	–	0.3
	v_{yz}	–	0.02
	v_{xz}	–	0.02
Density	ρ	kg/m^3	1600
Thickness	t	mm	0.3

Based on the four dimensionless variables (Eqs. (3)–(6)), the calculated results will be analyzed with two methods—independent variable J with parameter θ and independent variable θ with parameter J.

For the first method, J is an independent variable while θ is a parameter, and the T, Q, K_T, $10K_Q$, η will vary with J ranging from 0.3 to 0.7. The ARF angle θ varies through 11 steps (from −5 to +5° with an increment 1°, and when the ARF rotates to the suction surface it is defined that the rotation angle is negative, and vice

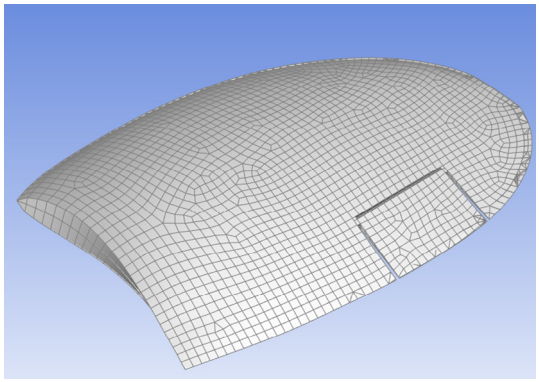

Fig. 9. The solid-based modeling composite blade.

versa). Similarly, for the second method, the T, Q, K_T, $10K_Q$, η will vary with θ ranging from -5 to $+5°$, and J is a parameter.

As shown in the Fig. 2(a) the flow field is composed of two parts i.e. inner flow field (IFF) and the other outer flow field (OFF). The IFF is the dynamic portion rotating around the propeller rotation axis to simulate the water passing through the propeller, and the OFF is stationary relative to the MCP. In Fluent, the multi-reference frame (MRF) model can realize this simulation process, and the Frame Motion option is selected for IFF, setting rotation velocity 900 rpm (15 rps), but the OFF stays stationary. Owing to the complex shape of the MCP configuration, hybrid mesh is utilized—the IFF is meshed with unstructured mesh and the OFF with structured mesh, illustrated in Fig. 2.

As discussed in Section 2, the standard $k-\varepsilon$ model was selected, for MCP performance analysis. For the open water simulation of the MCP, the velocity boundary condition is the crucial part, and 5 situations will be given — 1.08, 1.44, 1.80, 2.16, 2.52 m/s, the turbulent kinetic energy set to be 0.02 and turbulent dissipation rate to be 0.5; the stationary wall BC used for the cylinder surface of OFF, and the no-slip BC is utilized near the cylinder surface; the outflow BC is applied for the outlet and moving wall BC should be established for the MCP surface, and the moving type was rotational relative to the IFF. The pressure based solver was used and the pressure-velocity coupling was iterated with SIMPLE algorithm. Before the calculation procedure, an initialization must be given to initiate the solution so that the iteration can be proceeded.

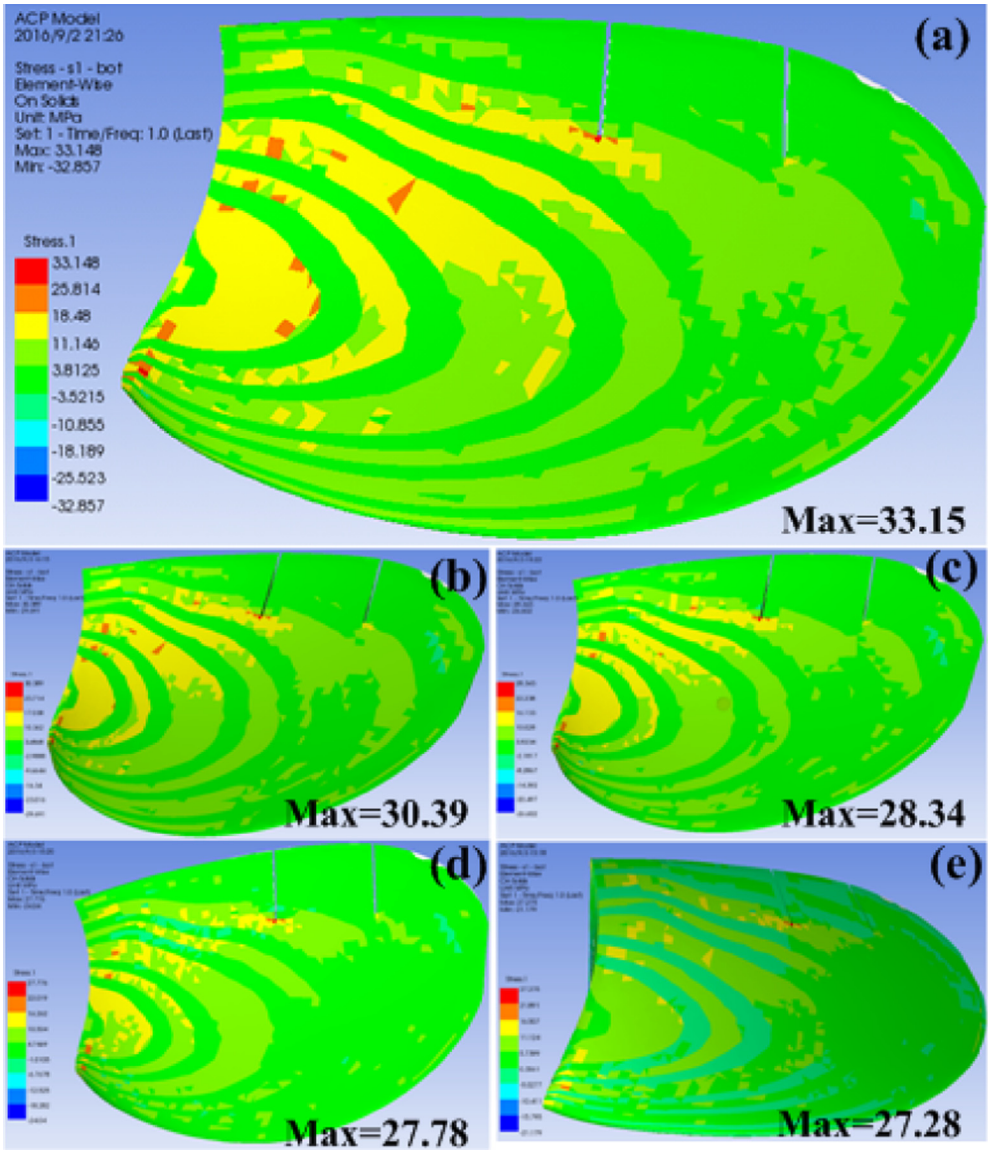

Fig. 10. The deformation contours of SS2 for the horizontal analysis (a)–(e) represent J = 0.3–0.7, respectively.

In Fluent simulation, advance speed V is the input variable and T, Q is obtained from the simulation results. Consequently, J, K_T, $10K_Q$, η can be calculated. For the open water simulation of the MCP, the parameter J has calculated for each angle of ARF. Two independent numerical analysis will be conducted for the change of ARF rotation and for the change of AC.

As shown in Fig. 3(a), the increase of AC J, each group of Thrust coefficient K_T linearly decreases at certain angle. At AC $J = 0.7$, a series of intersection points can be obtained, which can be treated as critical advance coefficients (J_{Tc}). As anticipated, J_{Tc} increases with the increase of θ, as the increase of θ will delay the initiation of negative thrust's. As such the rotation of ARF can adjust to control the adverse effect of the negative thrust under a constant rotation velocity of propeller shaft.

As shown in Fig. 3(b) when the AC J increases, the $10K_Q$ decreases at certain angle. Analogous to the thrust analysis, the torque analysis has something in common on the curves variation trend. Through the intercept on the J axis, the critical advance coefficient J_{Qc} can be obtained. The negative torque ($-Q$) will occur when $J > J_{Qc}$, and also, the J_{Qc} increases with the increase of θ due to the delayed "zero-Q".

With the increase of the AC J, the efficiency of the MCP climbs up to its maximum and then drops down dramatically. As shown in Fig. 3(c), the maximum efficiency is located in $J = 0.6$ for all curves and the value of each curve has an obvious distinction. Before $J = 0.6$, the efficiency for each curve increases. When $J = 0.7$, the efficiency increases with the increase of rotation angles at all the ACs, showing the positive effect of morphing composite propeller.

The three analyses above are the overall performance of the MCP, and some rules and trends are presented. This part details the local hydrodynamic forces acting on the MCP & ARF. The most critical property is the hydrodynamic force of apply on ARF i.e. flap thrust T_f. The T_f has obtained from the various AC Js under certain rotation angle θ. This data is essential for the design and fabrication of the TM. As depicted in Fig. 3(d), the T_f decreases linearly with the increase of J under various rotation angles θ ranging from $-5°$ to $+5°$. The slope of each curve decrease closer to horizontal state with the θ from $-5°$ to $+5°$. This phenomenon demonstrates that

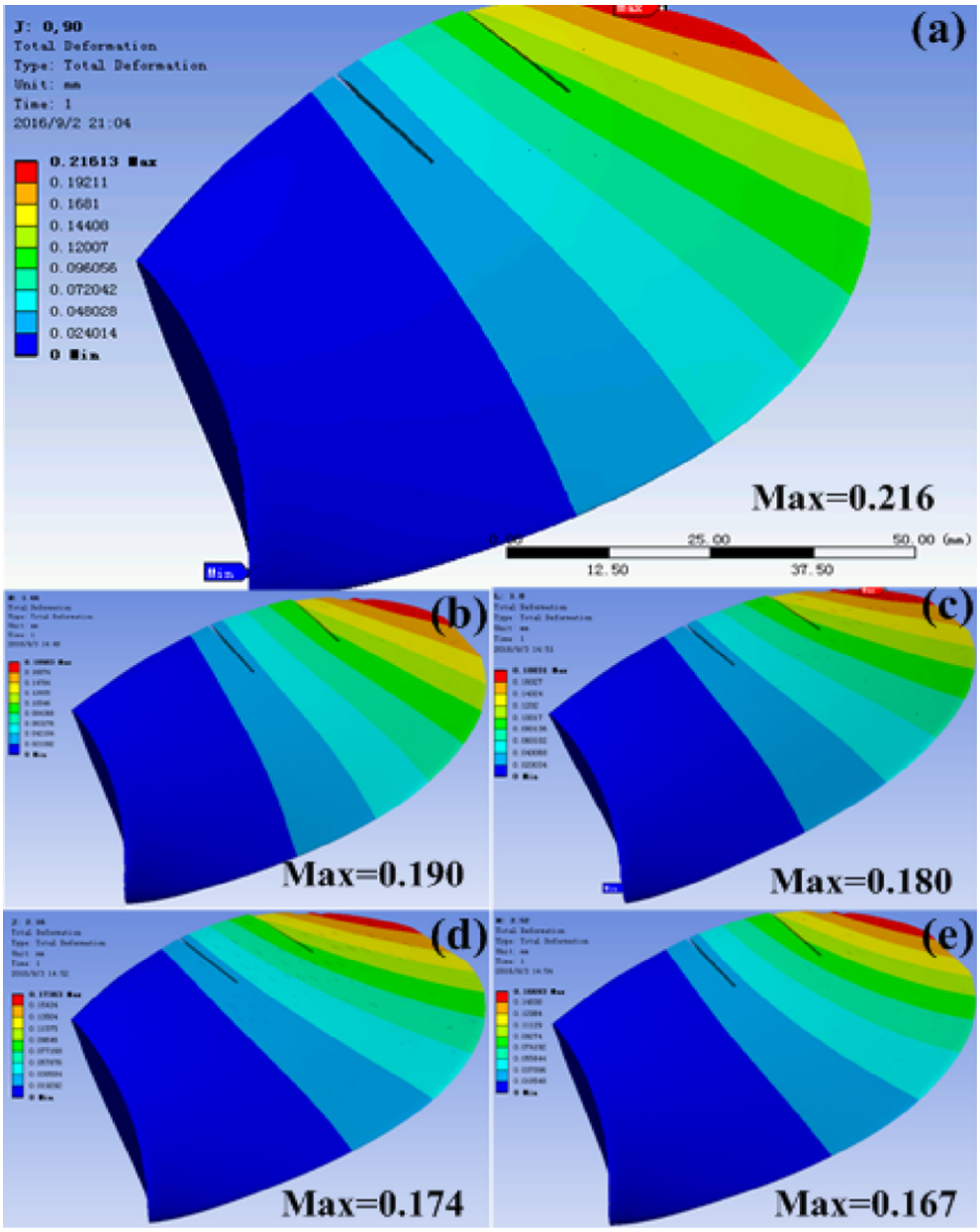

Fig. 11. The stress contours of SS2 for the horizontal analysis (a)–(e) represent $J = 0.3$–0.7, respectively.

the force acting on the ARF is significant with the change of inclination. The variation of T_f with the positive rotation of ARF seem to be less sensitive to the J's change compared to negative rotation. Therefore, positive rotation seems to be useful for improved advanced coefficient.

The analysis above is based on the first analysis method, namely, J to be independent variable and θ to be parameters. Following analysis details the second analysis method, that is, θ is an independent variable and J is a parameter.

As depicted in Fig. 4(a) with the increase of the rotation angle θ, under a certain AC J, K_T increases linearly. As such each curve can be approximate to a linear curve fitting. We can obtain the critical rotation angle θ_{Tc} through the intercept on the θ axis, which means, when $\theta < \theta_{Tc}$, the negative thrust ($-T$) of the MCP will occur. If the linear fitting is utilized and each curve is extended to left from the beginning of $\theta = -5°$, the θ_{Tc} of each curve crosses the θ axis within the range of $8.48° < |\theta_{Tc}| < 61.83°$. It can be observed that the $|\theta_{Tc}|$ decreases with the AC J increases, which means with J increase the rotation angle range narrowed down dramatically. However, for this work this effect is negligible as the rotation of ARF is relatively narrow range ($-5°$–$5°$).

As shown in Fig. 4(b), with a particular value of AC J, $10K_Q$ increases linearly with the increase of rotation angle θ. Analogous to the thrust on the MCP, the torque will be negative when the rotation angle $\theta < \theta_{Qc}$. And the range of the $|\theta_{Qc}|$ is from 15.16° to 52.03°. However, the actual case for the ARF is from $-5°$ to 5°, and therefore the negative case will not occur until a very large rotation angle ($\theta < -15°$).

With the increase of the rotation angle θ, the efficiency trend of the MCP can be divided into three cases (Fig. 4(c)):

Case 1: Efficiency decreases at $J = 0.3$;
Case 2: Efficiency is going up at $J = 0.4$ and down at 0.5,
Case 3: Efficiency increases at $J = 0.6$ and 0.7.

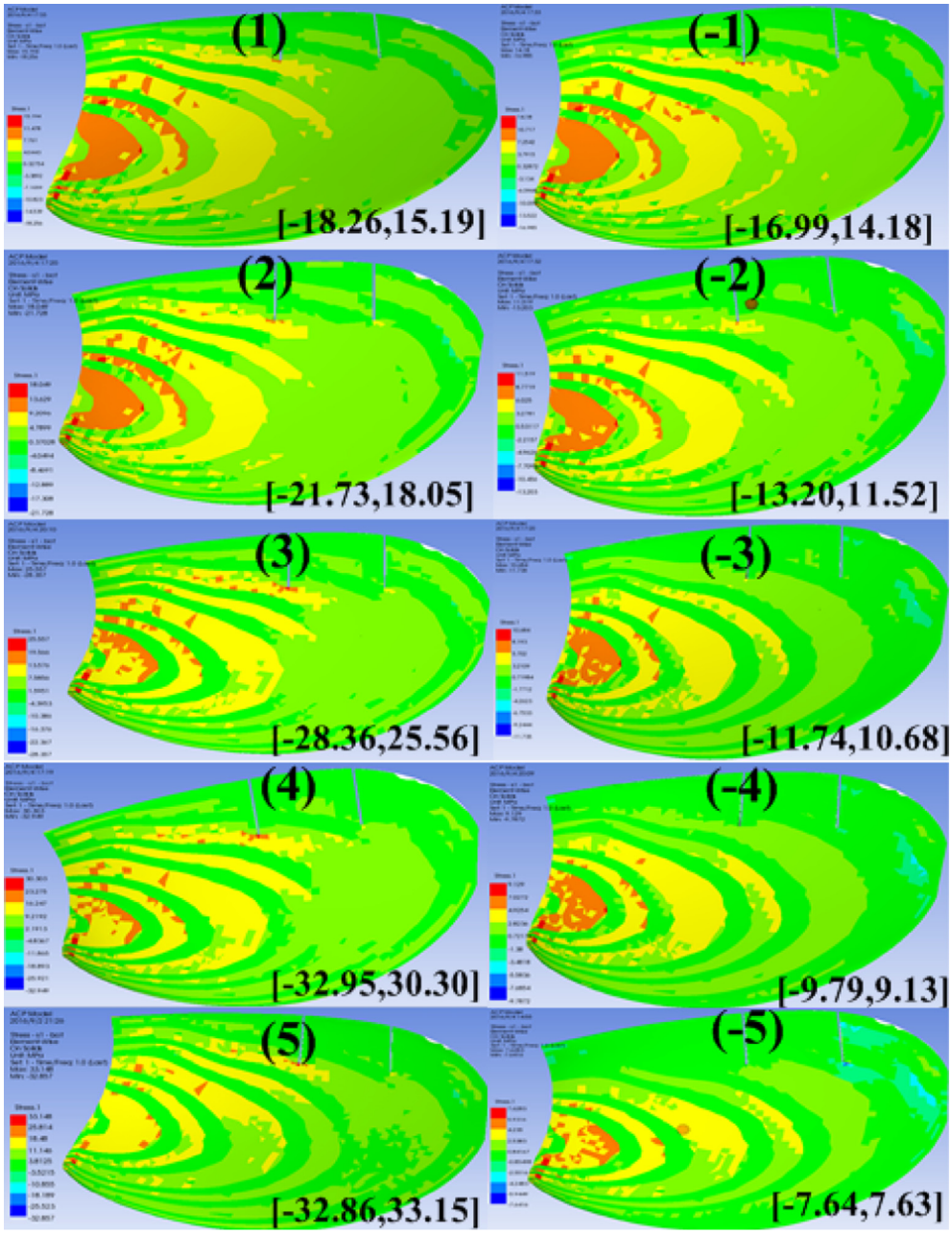

Fig. 12. The deformation contours with the rotation angles ranging from $-5°$ to +5°.

It is very obvious that the negative situation will not happen as the curve trend is relatively mild but one circumstance — $J = 0.7$. Under this advance coefficient, the negative value will present when θ reaches to $-6°$ or so, which is very close to $-5°$.

Further analysis was conducted to explore the thrust of the ARF (T_f) with the various values of AC J under a certain rotation angle. The thrust variation curves shown in Fig. 4(d). As shown in Fig. 4 (d), T_f increases linearly with the variation of rotation angle θs at AC J ranging from 0.3 to 0.7. However, the values of the T_f of different AC Js tend to be the same, especially when $\theta = 4°$ and $5°$. This phenomenon indicates that the T_f at rotation angles $\theta = 4°$ and $5°$ is less sensitive to the change of AC Js, as mentioned in a previous analysis.

5. The structural responses analysis of MCP under hydrodynamic pressure

For this section, two aspects will be analyzed. One is the influence assessment of the TM cavity of the MCP blade, and the other aspect is the structure response of the MCP based on the laminate stacking sequences. Compared with conventional materials for propeller manufacturing, composite materials have various merits, such as light weight, low acoustic emission, excellent designability etc.

For the modeling of MCP, it is a big trouble to stack the perfect MCP blade with TM cavity. Therefore, the suitable simplification is necessary to be proceeded. The following four parts will demonstrate the feasibility of our simplification ideas.

For structural analysis the aluminium alloy was selected to evaluate the influence with and without cavity. The geometry models are shown in Fig. 5(a) and (b), respectively. For comparison only one advanced speed 1.08 m/s is considered. The meshed models of the two propellers are shown in Fig. 5(c) and (d). The hydrodynamic pressure will be loaded on to the surfaces of the propeller models from Fluent analysis.

Figs. 6 and 7 shows displacement and stress of with and without cavity configurations respectively. The maximum displacement in the order of 1 mm both cases and the maximum stress is round 8 MPa and 15 MPa for without cavity and with cavity respectively. The maximum stresses levels due to the cavity is insignificant however the remaining area around the cavity is relatively thinner than other relevant areas. Therefore the cavity is redesigned shown as Fig. 8(a). The stress contour of the new design is shown in Fig. 8(b), and the maximum value is about 9 MPa, which seems sound and reasonable compared with 8 MPa.

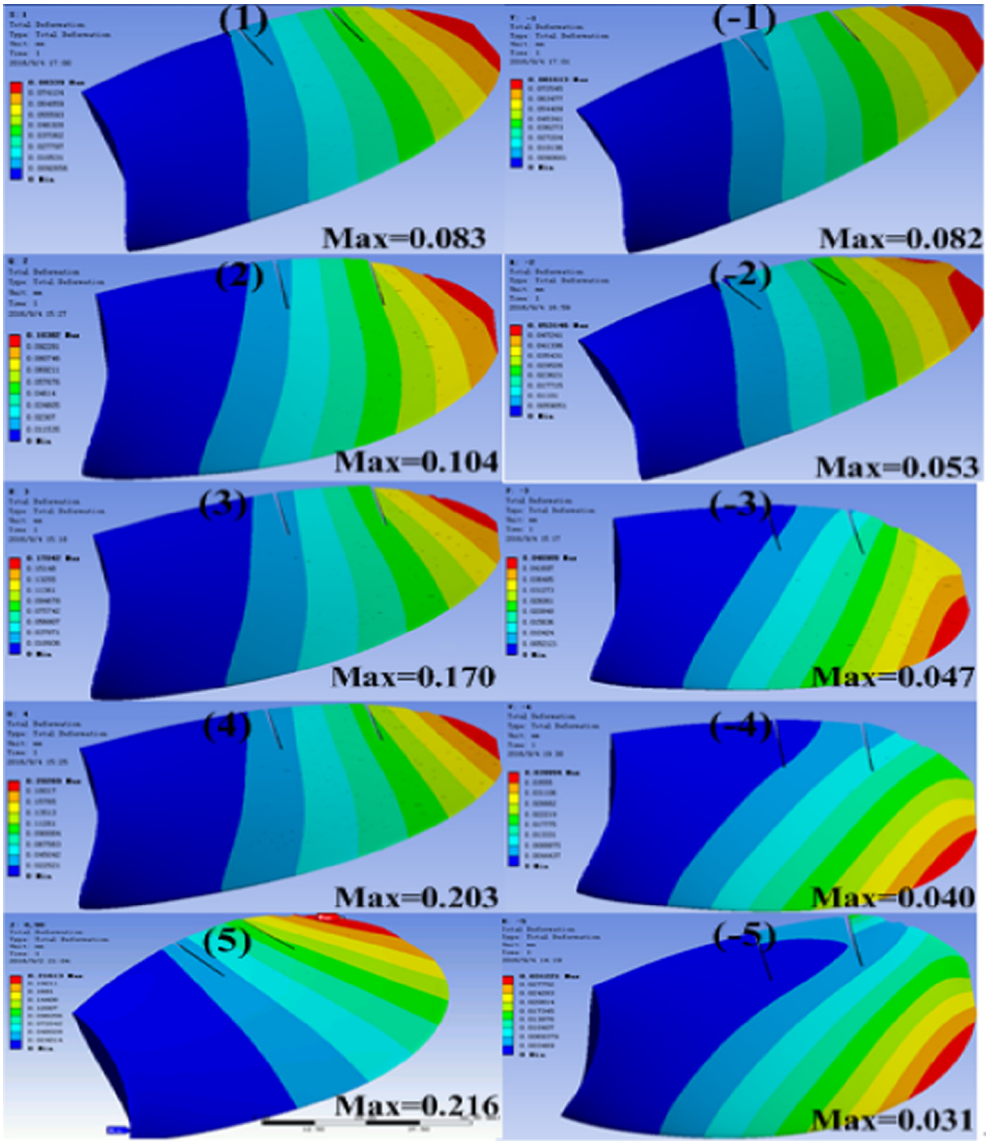

Fig. 13. The stress distributions with the rotation angles ranging from $-5°$ to $+5°$.

The structural responses for the blade with/wo cavity are calculated. The results show that blade without cavity (BWoC) and blade with cavity (BWC) have the similar structural responses and they can be replaced with each other (Table 1).

The composite analysis is based on a composite calculation module ACP PrepPost of ANSYS commercial software. Materials used is Uni-Directional Carbon Fibres and Epoxy matrix. Table 2 Shows a general material properties. Structural analysis for many trial laminate configurations were performed and finally 11 mm thick—$[0/90/0/90/0]_s$ configuration was selected. Following load cases were chosen as they represent the worst case scenarios.

1) For various AC *J*s at rotation angle being 5°, as the blade with 5° will acquires highest hydrodynamic loads under the same AC *J*;
2) The highest thrust and torque of AC $J = 1.08$ under various rotation angles θ from −5 to +5°.

As shown in Fig. 9, following assumptions have used for structural modeling process:

1) The ARF of the MCP blade will be unchangeable, with its rotation angle being 0°;
2) The ARF is a part/area of the blade instead of connecting on the blade;
3) The slots on the blade represent the gaps between ARF and blade.

FEA analysis has shown the deformation and strength aspects for the 2 cases aforementioned. For the first case (Figs. 10 and 11), the maximum stresses of the blade undergo from 27.28 MPa to 33.15 MPa and the maximum displacements from 0.167 mm to 0.216 mm. For the second case, shown in Figs. 12 and 13, the maximum stresses (both negative values and positive values) of the blade undergo from −7.64 MPa to −32.95 MPa for negative values and 7.63 MPa to 33.15 MPa for positive values and the maximum displacements from 0.031 mm to 0.216 mm. The reason to demonstrate this phenomenon can also attribute to the hydrodynamics increase with rotation angles. The hydrodynamics increase will bring about the larger negative and positive stress responses.

6. Conclusions

This paper introduces a novel morphing composite propeller blade with improved efficiency and less acoustic emission. A detailed hydrodynamics and structural analysis is presented. Embracing the morphing concept, several facets of the issues have been investigated: (1) the MCP system is designed and assembled with its components designed and optimized. (2) The MCP's hydrodynamic response is critically analyzed. The results shows that rotation of ARF significantly influence the MCP's hydrodynamic response and found the best range of rotation is from −5° to +5°. The thrust and torque linearly increase and the efficiency varies with different ACs. The simplified MCP blade is designed with Carbon Fibre/Epoxy laminates and found its structural response is as same as its counterpart metallic materials.

Acknowledgment

This work is supported by the National Natural Science Foundation of China (Grant No. 11225211).

References

[1] Bandyopadhyay PR, Krol WP, Thivierge DP, Nedderman WH, Mojarrad M. A biomimetic propulsor for active noise control. Part 1: experiments. Bull Am Phys Soc 2000;45(9).
[2] Annaswamy M, Krol WP, Bandyopadhyay PR. A biomimetic propulsor for active noise control. Part 2: theory. Bull Am Phys Soc 2000;45(9).
[3] Wasylyszyn Jonathan Allen. Active control of underwater propulsor using shape memory alloys [Master Dissertation]. Texas A&M University; 2005.
[4] Stern F, Kim HT, Patel VC, Chen HC. A viscous-flow approach to the computation of propeller-hull interaction. J Ship Res 1988;32(4):246–62.
[5] Abdel-Maksoud M, Menter F, Wuttke H. Viscous flow simulations for conventional and high-skew marine propellers. Ship Technol Res 1998;45(2):64–71.
[6] Rhee SH, Joshi S. CFD validation for a marine propeller using an unstructured mesh based RANS method. In: Proceedings of FEDSM, USA.
[7] Brogliaa Riccardo, Dubbiosoa Giulio, Durantea Danilo, Di Masciob Andrea. Simulation of turning circle by CFD: analysis of different propeller models and their effect on manoeuvring prediction. Appl Ocean Res 2012;39:1–10.
[8] Gaggero Stefano, Tani Giorgio, Viviani Michele, Conti Francesco. A study on the numerical prediction of propellers cavitating tip vortex. Ocean Eng 2014;92:137–61.
[9] Sánchez-Caja, Martio J, Saisto I, Siikonen T. On the enhancement of coupling potential flow models to RANS solvers for the prediction of propeller effective wakes. J Mar Sci Technol 2015;20:104–17.
[10] Ji Bin, Luo Xianwu, Wu Yulin, Peng Xiaoxing, Xu Hongyuan. Partially-Averaged Navier-Stokes method with modified k–e model for cavitating flow around a marine propeller in a non-uniform wake. Int J Heat Mass Transf 2012;55:6582–8.
[11] Lin HJ, Lin JJ. Nonlinear hydroelastic behavior of propellers using a finite element method and lifting surface theory. J Mar Sci Technol 1996;1:114–24.
[12] Lin HJ, Lin JJ. Effect of stacking sequence on the hydroelastic behavior of composite propeller blades. In: Eleventh international conference on composite materials, Gold Coast, Australia: Australian Composite Structures Society; 1997.
[13] Lee YJ, Lin CC. Optimized design of composite propeller. Mech ASC Adv Mater Struct 2004;11:17–30.
[14] Lin HJ, Lin JJ. Strength evaluation of a composite marine propeller blade. J Reinf Plast Compos 2005;24:1791–807.
[15] Young YL. Time-dependent hydroelastic analysis of cavitating propulsors. J Fluids Struct 2007;23:269–95.
[16] Young YL. Fluid-structure interaction analysis of flexible composite marine propellers. J Fluids Struct 2008;24:799–818.
[17] Motley MR, Liu Z, Young YL. Utilizing fluid–structure interactions to improve energy efficiency of composite marine propellers in spatially varying wake. Compos Struct 2009;90:304–13.
[18] Young YL. Dynamic hydroelastic scaling of self-adaptive composite marine rotors. Compos Struct 2010;92:97–106.
[19] Young YL, Baker JW, Motley MR. Reliability-based design and optimization of adaptive marine structures. Compos Struct 2010;92:244–53.
[20] Nelsona M, Temple DW, Hwangb JT, Young YL, Martinsb JRRA, Collette M. Simultaneous optimization of propeller – hull systems to minimize lifetime fuel consumption. Appl Ocean Res 2013;43:46–52.
[21] Martins P, Lopes AC, Lanceros-Mendez S. Electroactive phases of poly (vinylidene fluoride): determination, processing and applications. Prog Polym Sci 2014;39:683–706.
[22] Yi Guo, Wang Jinming, Liu Liwu, Liu Yanju, Leng Jinsong. Active vibration control of basic structures using macro fiber composites. Proceedings of SPIE 2011;7977:79772C.
[23] Gao Le, Qingqing Lu, Fei Fan, Liu Liwu, Liu Yanju, Leng Jinsong. Active vibration control based on piezoelectric smart composite. Smart Mater Struct 2013;22:125032.
[24] Karunanidhi S, Singaperumal M. Design, analysis and simulation of magnetostrictive actuator and its application to high dynamic servo valve. Sens Actuators A 2010;157:185–97.
[25] Grunwald A, Olabi AG. Design of a magnetostrictive (MS) actuator. Sens Actuators A 2008;144:161–75.
[26] Feng Ning, Liu Liwu, Liu Yanju, Leng Jinsong. Characteristics of multi-functional composites using elastomer embedded with Shape Memory Alloy wires. Mater Des 2015;88:75–81.
[27] Zhou B, Liu YJ, Leng JS. A constitutive model for shape memory alloy in pure shear state. Acta Metall Sin 2009;45(10):1179–84.
[28] Leng Jinsong, Lan Xin, Liu Yanju, Shanyi Du. Shape-memory polymers and their composites: stimulus methods and applications. Prog Mater Sci 2011;56:1077–135.
[29] Liu Yanju, Du Haiyang, Liu Liwu, Leng Jinsong. Shape memory polymers and their composites in aerospace applications: a review. Smart Mater Struct 2014;23:023001.
[30] Du Haiyang, Liu Liwu, Leng Jinsong, Peng Huaxin, Scarpa Fabrizio, Liu Yanju. Shape memory polymer S-shaped mandrel for composite air duct manufacturing. Compos Struct 2015;133:930–8.
[31] Liu Liwu, Liu Yanju, Kai Yu, Leng Jinsong. Thermoelectromechanical stability of dielectric elastomers undergoing temperature variation. Mech Mater 2014;72:33–45.
[32] Liu Liwu, Kai Yu, Liu Yanju, Leng Jinsong. Polar elastic dielectric of large electrocaloric effect and deformation. Mech Mater 2014;69:71–92.
[33] Chopra Inderjit. Status of application of smart structures technology to rotorcraft systems. J Am Helicopter Soc 2000;45(4):228–52.
[34] Lee Taeoh, Chopra Inderjit. Design of piezo-stack-driven trailing-edge flap actuator for helicopter rotors. Smart Mater Struct 2001;10:15–24.
[35] Andreas PF, Bernhard, Chopra Inderjit. Hover testing of an active rotor blade tip and structural analysis of the actuator beam. In: 39th AIAA/ASME/ASCE/

AHS/ASC Structures, structural dynamics and materials conference and AIAA/AME/AHS adaptive structures forum, Longbeach, CA.
[36] Straub Friedrich K, Kennedy Dennis K, Stemple Alan D, Anand VR, Birchette Terry S. Development and whirl tower test of the SMART active flap rotor. Proceedings of SPIE 2004;5388:202–12.
[37] Lu Qingqing. Helicopter active trailing-edge flap with piezoelectric actuator [Master Dissertation]. China: Harbin Institute of Technology; 2013.
[38] Versteeg HK, Malalasekera W. An introduction to computational fluid dynamics: the finite volume method. New York: Wiley; 1995.
[39] Blasques Jose Pedro, Berggreen Christian, Andersen Poul. Hydroelastic analysis and optimization of a composite marine propeller. Mar Struct 2010;23(1):22–38.